

# Hybrid Tendon and Ball Chain Continuum Robots for Enhanced Dexterity in Medical Interventions

Giovanni Pittiglio<sup>1</sup>, Margherita Mencattelli<sup>1</sup>, Abdulhamit Donder<sup>1</sup>, Yash Chitalia<sup>2</sup>, and Pierre E. Dupont<sup>1</sup>

**Abstract**—A hybrid continuum robot design is introduced that combines a proximal tendon-actuated section with a distal telescoping section comprised of permanent-magnet spheres actuated using an external magnet. While, individually, each section can approach a point in its workspace from one or at most several orientations, the two-section combination possesses a dexterous workspace. The paper describes kinematic modeling of the hybrid design and provides a description of the dexterous workspace. We present experimental validation which shows that a simplified kinematic model produces tip position mean and maximum errors of 3% and 7% of total robot length, respectively.

**Index Terms**—Medical Robots and Systems, Steerable Catheters, Flexible Robotics, Magnetic Actuation, Continuum robots.

## I. INTRODUCTION

Continuum robots have attracted considerable attention for applications in minimally invasive diagnostics and therapeutics over the past decade [1]. The primary reason is their ability to navigate narrow and tortuous anatomical passageways, while safely interacting with the anatomy.

In designing such robots, an important goal is to create a robot with a workspace appropriate for the clinical task. A significant limitation of many continuum designs is that these robots lack a dexterous workspace. While clinical applications may necessitate approaching a target with a specific angle of approach, continuum designs are often limited in this regard. Furthermore, while multiple bending sections can be concatenated to provide more degrees of freedom, the orientations by which a point in the workspace can be approached are often highly constrained.

To overcome this limitation, this paper investigates a hybrid design that combines the advantages of tendon actuation [2] and magnetic ball chain robots [3], [4] as shown in Fig. 1. In this hybrid design, a proximal tendon-actuated section positions the robot with respect to the goal tip location while a distal ball chain section orients the robot tip via an externally-produced magnetic field.

This hybrid design is perhaps the only two section continuum robot possessing a true dexterous workspace - a continuous set of tip positions that can be approached from an arbitrary direction.

<sup>1</sup>Department of Cardiovascular Surgery, Boston Children's Hospital, Harvard Medical School, Boston, MA 02115, USA. Email: {giovanni.pittiglio, margherita.mencattelli, abdulhamit.donder, pierre.dupont}@childrens.harvard.edu

<sup>2</sup>Department of Mechanical Engineering, University of Louisville, Louisville, KY 40292, USA. yash.chitalia@louisville.edu This work was supported by the National Institutes of Health under grant R01HL124020.

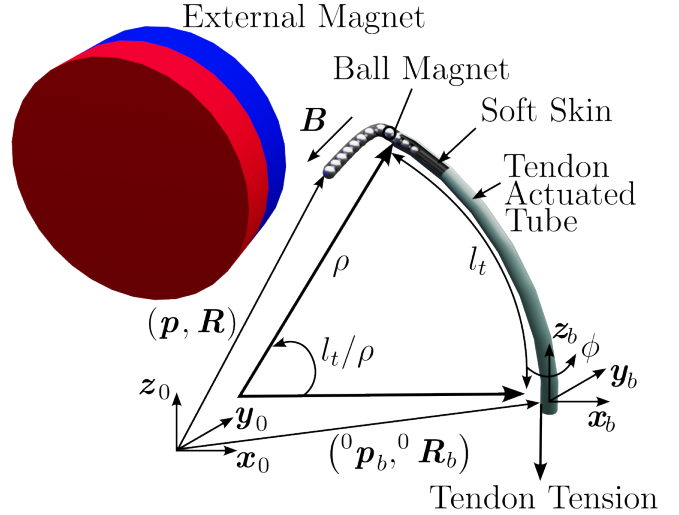


Fig. 1: Hybrid robot comprised of proximal tendon-actuated section and distal telescoping magnetic ball-chain section.

The remainder of the paper is arranged as follows. The next two sections describe how kinematic models of varying complexity can be constructed for the tendon- and magnetically-actuated design. The subsequent section uses an approximate kinematic model to characterize the dexterous workspace. Section V contains an experimental validation of the kinematic model and workspace. Conclusions appear in the final section.

## II. KINEMATIC MODELING

A complete mechanics-based model of the hybrid design can be derived by combining the tendon-actuated model of [2] with the magnetic energy ball-chain model of [3], [4]. In this approach, the magnetic balls retracted inside the tendon-actuated tube exert “external” point loads on the tube while the extended portion of the ball chain exerts a tip force on the tube. The magnitudes of these forces can be computed using the formulation of [3], but depend on the deflected tube shape. An iterative approach can be used to alternately solve the tube and ball chain models until convergence is reached.

If the forces from the magnetic ball chain do not appreciably deflect the tendon-actuated tube, the kinematic modeling equations and solution procedure can be substantially simplified and solved in a single iteration. In this case, the tendon-actuated tube shape can be computed first. The position constraints from the tube shape can then be imposed on the ball chain to solve for the shape of its extended portion. When this simplification can be applied, it is advantageous

since the model becomes less complex and the computation time faster. Because of these advantages, we investigate the simplified model in this paper. The following subsections summarize the tendon-actuated tube model and the magnetic energy ball chain model.

#### A. Tendon-actuated tube

The centerline of the tube can be described, as a function of arc-length,  $s \in [0, l_t]$ , with its position  $\mathbf{p}_c(s) \in \mathbb{R}^3$  and orientation  $\mathbf{R}_c(s) \in SO(3)$ ,

$$\dot{\mathbf{p}}_c(s) = \mathbf{R}_c(s)\mathbf{v}(s) \quad (1a)$$

$$\dot{\mathbf{R}}_c(s) = \mathbf{R}_c(s)\mathbf{u}_\times(s) \quad (1b)$$

where  $\mathbf{v}(s) \in \mathbb{R}^3$  and  $\mathbf{u}(s) \in \mathbb{R}^3$  are the respective linear and angular strain; the ‘‘skew’’ operator is defined as  $\mathbf{u}_\times = (\mathbf{u} \times \mathbf{e}_1 \ \mathbf{u} \times \mathbf{e}_2 \ \mathbf{u} \times \mathbf{e}_3)$  with  $\mathbf{e}_i \in \mathbb{R}^3$   $i$ th element of the canonical basis of  $\mathbb{R}^3$ ,  $\times$  indicating the cross product. Here, the dot notation is used to indicate derivatives with respect to arc-length (i.e.  $\dot{\mathbf{p}}_c(s) = \frac{d\mathbf{p}_c(s)}{ds}$ ). Following the Cosserat rod modeling [2], we describe the internal forces  $\mathbf{n}$  and moments  $\mathbf{m}$  with respect to the applied force  $\mathbf{f}$  and torque  $\boldsymbol{\tau}$  as

$$\begin{pmatrix} \dot{\mathbf{n}} \\ \dot{\mathbf{m}} \end{pmatrix} = \begin{pmatrix} \mathbf{u}_\times & \mathbf{0} \\ \mathbf{v}_\times & \mathbf{u}_\times \end{pmatrix} \begin{pmatrix} \mathbf{n} \\ \mathbf{m} \end{pmatrix} + \begin{pmatrix} \mathbf{f} \\ \boldsymbol{\tau} \end{pmatrix} \quad (2)$$

Under assumption of linear elasticity, we have

$$\begin{pmatrix} \mathbf{n} \\ \mathbf{m} \end{pmatrix} = K \begin{pmatrix} \mathbf{u} - \mathbf{u}_0 \\ \mathbf{v} - \mathbf{v}_0 \end{pmatrix} \quad (3)$$

with  $K = \text{diag}(GA, GA, EA, EI_{xx}, EI_{yy}, GJ_{zz})$ , where  $G$  is the shear modulus,  $E$  modulus of elasticity,  $A$  cross-sectional area,  $I_{xx}$ ,  $I_{yy}$  second moment of area around the  $\mathbf{x}$  and  $\mathbf{y}$  axes, and  $J_{zz}$  the polar moment of area;  $\mathbf{u}_0$  and  $\mathbf{v}_0$  are the initial angular and linear strain respectively.

The tube is subject to two main external inputs: distributed force related to the force applied by the tendon at the tip  $\mathbf{f}_t$ ; and gravitational force  $\mathbf{f}_g = m\mathbf{g}$ ,  $m$  mass density and  $\mathbf{g}$  gravitational acceleration.

Following [2], the path of the tendon on the surface of the tube along the  $\mathbf{x}$  axis is

$$\mathbf{p}_t(s) = \mathbf{p}_c(s) + \frac{d_t}{2} \mathbf{R}_c(s)\mathbf{e}_1 \quad (4)$$

and the relative force and torque are

$$\mathbf{f}_t = -\lambda \frac{\dot{\mathbf{p}}_{t \times}^2}{\|\mathbf{p}_t\|^3} \ddot{\mathbf{p}}_t \quad (5a)$$

$$\boldsymbol{\tau}_t = \mathbf{p}_t \times \mathbf{f}_t \quad (5b)$$

with  $\lambda$  tension applied to the tendon and  $d_t$  is the diameter of the tube.

The load at the tip is implemented as a boundary condition,

$$\mathbf{F}(l_t) = -\lambda \frac{\dot{\mathbf{p}}_c(l_t)}{\|\dot{\mathbf{p}}_c(l_t)\|} \quad (6a)$$

$$\mathbf{T}(l_t) = (\mathbf{p}_c(l_t) - \mathbf{p}_t(l_t)) \times \mathbf{F}(l_t). \quad (6b)$$

#### B. Magnetic ball chain

The equilibrium configuration of the magnetic ball chain can be solved by minimizing the potential energy of the system. Following [3], [5], the total potential energy of the balls can be expressed as a combination of magnetic and gravitational components as

$$U_e = - \sum_{i=1}^n \boldsymbol{\mu}_i \cdot \mathbf{B}(\mathbf{p}_i - \mathbf{p}_e, \boldsymbol{\mu}_e) \quad (7a)$$

$$U_b = - \sum_{i=1}^n \sum_{j=i+1}^n \boldsymbol{\mu}_i \cdot \mathbf{B}(\mathbf{p}_i - \mathbf{p}_j, \boldsymbol{\mu}_j) \quad (7b)$$

$$U_g = \sum_{i=1}^n m_i \mathbf{g}^T \mathbf{p}_i, \quad (7c)$$

In (7a), we express the interaction with the external magnet in position  $\mathbf{p}_e$  and magnetic dipole  $\boldsymbol{\mu}_e$ , (7b) considers the intermagnet energy for the magnets in the chain, and (7c) is the gravitational component. The magnetic field is computed using the dipole model

$$\mathbf{B}(\mathbf{r}, \boldsymbol{\mu}) = \frac{\mu_0}{4\pi|\mathbf{r}|^3} \left( 3\hat{\mathbf{r}}\hat{\mathbf{r}}^T - \mathbf{I} \right) \boldsymbol{\mu}.$$

By combining the terms in (7), we obtain the total energy  $U = U_e + U_b + U_g$ . In [3], we have considered the discrete nature of the chain and discretized the radius of curvature  $\rho_i$  and bending angle  $\theta_i$  (see Fig. 2) between consecutive balls, to consider elastic terms in the sleeve containing the chain. In contrast to our prior work, we solve for the minimum energy configuration while constraining the position of the  $n_i$  balls inside the tube using Matlab function *fmincon*, since the tube can be considered infinitely stiff, in this case. These constraints are given by

$$\mathbf{p}_i = \mathbf{p}_{i_0} \ \forall i = 1, 2, \dots, n_i \quad (8)$$

$\mathbf{p}_{i_0}$  is derived from the the Cosserat equilibrium.

As in our previous work [5], we constrain each ball to be in continuous contact with the previous one and the dipole intensity of the  $n$  balls to be constant

$$\|\mathbf{p}_i - \mathbf{p}_{i-1}\| = d \ \forall i = 2, 3, \dots, n. \quad (9a)$$

$$\|\boldsymbol{\mu}_i\| = \mu \ \forall i = 1, 2, \dots, n. \quad (9b)$$

The overall solution is obtained by first solving for the shape of the tendon-actuated tube and then using its position to solve for the shape of the ball chain.

### III. CLOSED-FORM KINEMATICS

In the prior section, a kinematic model was derived under the assumption that the ball chain does not deflect the proximal tendon-actuated tube. Even with this assumption, solution of the model involves solving a two-point boundary value problem and a constrained energy minimization problem. For purposes of design, workspace analysis and initialization of more complicated models, it is convenient to have a closed-form solution for the kinematics.

We present such a model by making two additional simplifications. First, as explained in [2], the constant-curvature

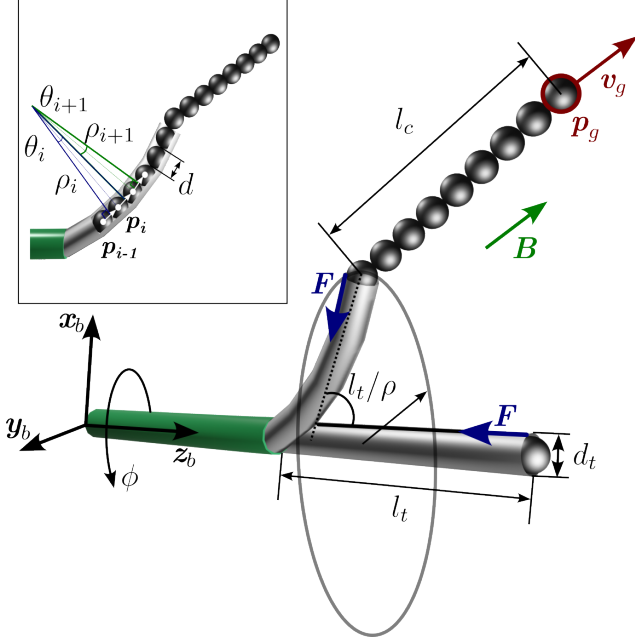


Fig. 2: Hybrid model parameters. Proximal section,  $l_t$ , is assumed constant curvature with radius of curvature  $\rho$  under tension  $F$ . Extended ball chain,  $l_c$ , is assumed linear in field direction  $\mathbf{B}$ .

model for a tendon-actuated tube in which the tendon load is approximated as a point moment at the tip is as accurate as the model of [2] for cases of no external load or loads applied in the plane of bending. This condition is satisfied based on our initial no-coupling assumption.

Second, as noted in [5], the ball chain assumes a nearly linear shape aligned with the external magnetic field for sufficiently high field strengths. Under this assumption, it is possible to derive approximate closed-form forward and inverse kinematic models, as described below.

#### A. Forward Kinematics

The following notation is graphically explained in Fig. 1. A ball chain robot is assumed to extend, for a length  $l_c = nd_c$ , as a straight line; here  $n$  is the number of balls and  $d_c$  their diameter. Given their base position and orientation in global reference frame,  ${}^0\mathbf{p}_b$  and  ${}^0\mathbf{R}_b$ , their tip position and orientation is

$$\mathbf{p} = {}^0\mathbf{p}_b + nd_c {}^0\mathbf{R}_b\boldsymbol{\omega} \quad (10a)$$

$$\mathbf{R} = {}^0\mathbf{R}_b \exp(\boldsymbol{\omega}_\times). \quad (10b)$$

The direction of the chain is a vector of norm 1,  $\boldsymbol{\omega} = \hat{\mathbf{B}} = \mathbf{B}/\|\mathbf{B}\|$ , and  $\exp(\boldsymbol{\omega}_\times)$  the matrix exponential of  $\boldsymbol{\omega}_\times$ . We approximate the tendon-actuated continuum robot using constant curvature assumption,

$$\mathbf{p} = {}^0\mathbf{p}_b + {}^0\mathbf{R}_b \text{rot}_{\mathbf{e}_3}(\phi)\mathbf{w} \quad (11a)$$

$$\mathbf{R} = {}^0\mathbf{R}_b \text{rot}_{\mathbf{e}_3}(\phi) \text{rot}_{\mathbf{e}_2}\left(\frac{l_t}{\rho}\right) \quad (11b)$$

with  $\mathbf{w} = \rho(1 - \cos(l_t/\rho) \ 0 \ \sin(l_t/\rho))^T$ ,  $\rho$  and  $l_t$  respective radius of curvature and length of the tendon-actuated continuum robot;  $\text{rot}_{\mathbf{e}_i}(\delta)$  is the rotation of the angle  $\delta$  around the axis  $\mathbf{e}_i$ .

By combining (10) with (11), we obtain the kinematics of the hybrid robot

$$\mathbf{p} = {}^0\mathbf{p}_b + {}^0\mathbf{R}_b \text{rot}_{\mathbf{e}_3}(\phi)\mathbf{w} + nd_c \text{rot}_{\mathbf{e}_2}(\beta)\boldsymbol{\omega} \quad (12a)$$

$$\mathbf{R} = {}^0\mathbf{R}_b \exp(\boldsymbol{\omega}_\times) \quad (12b)$$

Notice that, for any orientation of the tip of the tendon-actuated portion, the orientation of the chain's tip is dictated by the magnetic field direction.

#### B. Inverse Kinematics

The inverse kinematics problem is to solve for the set of inputs  $\{F, \phi, \hat{\mathbf{B}}\}$  for which the last ball of the chain approaches a goal position  $\mathbf{p}_g$  with orientation  $\mathbf{v}_g$  (see Fig. 2). The input  $F$  refers to the pulling force applied to the tendon,  $\phi$  is the angular rotation around the main axis  $\mathbf{z}_b$ , and  $\hat{\mathbf{B}}$  is the field direction.

First, we guarantee that the objective is feasible, i.e. we check if the point is reachable and the approach angles are within range. The distance from the axis is computed as  $r = \sqrt{p_{g_x}^2 + p_{g_y}^2}$ , and has to guarantee  $r \leq r_d + nd_c$ . The goal angle  $\alpha_g$  and  $\beta_g$  can be found as the twice the angle between  $\mathbf{v}_g$  and the respective axes  $\mathbf{e}_2$  and  $\mathbf{e}_3$ :  $\alpha_g = 2 \arctan(\mathbf{v}_g \cdot \mathbf{e}_2 / \|\mathbf{v}_g \times \mathbf{e}_2\|)$  and  $\beta_g = 2 \arctan(\mathbf{v}_g \cdot \mathbf{e}_3 / \|\mathbf{v}_g \times \mathbf{e}_3\|)$ . If  $\alpha_g \leq \alpha_M(r)$  and  $\beta_g \leq \beta_M(r)$ , the inverse kinematics can be solved. The maximum range of orientations is defined in the next section.

To solve for the tendon-actuated section, we search for the intersection between a line (the ball chain), extending from  $\mathbf{p}_g$  in the direction  $-\mathbf{v}_g$ , and the cylinder of axis  $\mathbf{e}_3$  and radius  $r_c$ :

$$\begin{cases} \mathbf{p}(s) & = \mathbf{p}_g - \mathbf{v}_g s \\ p_x^2(s) + p_y^2(s) & \leq r_d^2 \\ \|\mathbf{v}_g s\| & \leq nd_c \end{cases} \quad (13)$$

which also satisfies

$$\begin{cases} A - B & \leq s \leq A + B \\ & s \leq \frac{nd_c}{\|\mathbf{v}_g\|} \end{cases} \quad (14)$$

where

$$A = \frac{-p_{g_x} v_{g_x} + p_{g_y} v_{g_y}}{v_{g_x}^2 + v_{g_y}^2} \quad (15a)$$

$$B = \frac{\sqrt{-(p_{g_x} v_{g_x} + p_{g_y} v_{g_y})^2 - r_d^2 (v_{g_x}^2 + v_{g_y}^2)}}{v_{g_x}^2 + v_{g_y}^2} \quad (15b)$$

We can select any  $s^*$  satisfying (15) and find the intersection point  $\mathbf{p}_i = \mathbf{p}(s^*)$ .

We convert  $\mathbf{p}_i$  into cylindrical coordinates to find  $\phi = \arctan(p_{i_y}/p_{i_x})$  and, from the direct kinematics in (11), we impose  $\rho(1 - \cos(l_t/\rho)) = p_{i_x}$  and obtain  $\rho = p_{i_x}/(1 - \cos(k))$ , for some  $k > 0$ . Assuming constant curvature, the moment at the tip of the tube is  $\mathbf{m} = EI/\rho \mathbf{e}_2$ , and by applying the force  $F$  along the surface of the robot, we

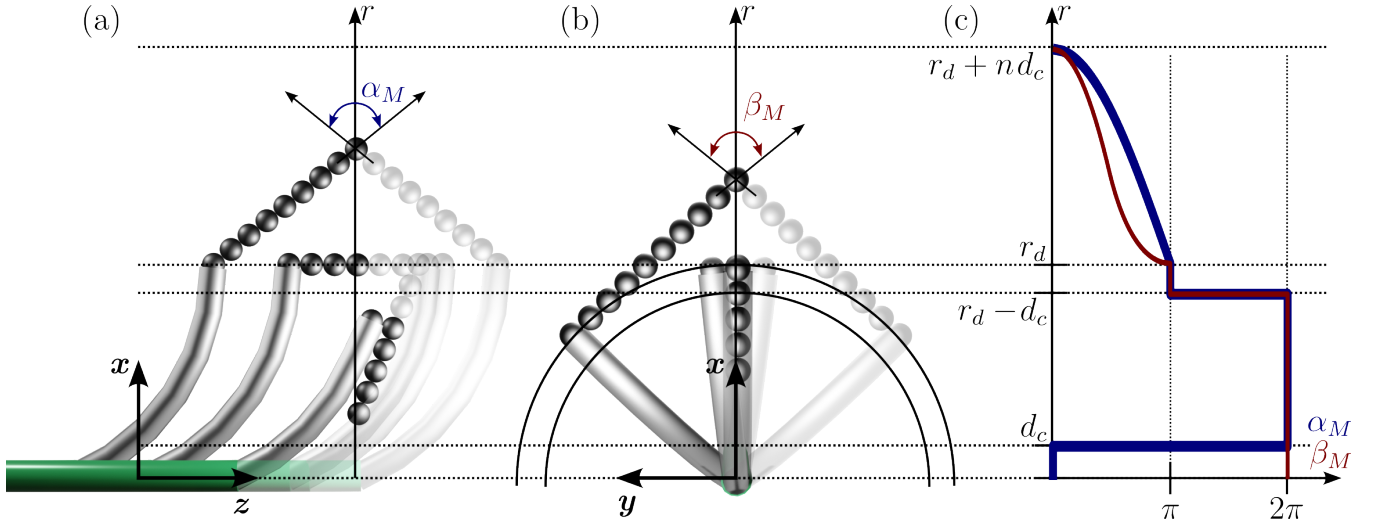


Fig. 3: Dexterous workspace. (a) Side view orientation angle range,  $\alpha_M$ , as function of  $x$ . (b) Front view orientation angle,  $\beta_M$ , as function of  $x$ . (c)  $\alpha_M$  and  $\beta_M$  as a function of  $x$ . Dexterous workspace lies in range  $d_c \leq x \leq r_d - d_c$

obtain the equilibrium  $Fd/2e_2 = -EI/\rho e_2$  and find the tendon force to be

$$F = -\frac{2EI(1 - \cos(k))}{dp_{i_x}}. \quad (16)$$

The constant  $k$  is constrained by the inserted length of the robot, depending on the anatomical site, and the amount of tension which can be applied to the tendon. These considerations are fundamental in the design for application-specific catheters.

#### IV. DEXTEROUS WORKSPACE CHARACTERIZATION

In Fig. 3, we describe the dexterous workspace of the hybrid design, derived from (12), in the  $x-z$  plane in Fig. 3(a) and in the  $x-y$  plane in Fig. 3(b). Figure 3(c) depicts the range of approach angles that the hybrid robot can achieve with respect to the radial distance  $r$ , from the  $z$  axis. The achievable robot tip tangent directions are described in terms of the allowable angle ranges  $\alpha_M$  about the  $y$  axis in the  $x-z$  plane, and  $\beta_M$  about the  $z$  axis in the  $x-y$  plane.

Full dexterity occurs when  $\alpha_M = \beta_M = 2\pi$ . As shown in Fig. 3(c), this is true in the range  $d_c < r < r_d - d_c$ . Here, we consider the center of the distal ball to be the robot tip. The distance  $r_d$  corresponds to the radius of curvature of the steerable sheath when its tip is deflected by  $\pi/2$ . If the maximum deflection of the sheath is less than  $\pi/2$  then  $r_d$  is given by its maximum radial deflection.

In the range  $r_d - d_c \leq r \leq r_d$ , the ball chain cannot achieve tangent directions pointing downward and so  $\alpha_M = \beta_M = \pi$ .

For  $r > r_d$ , the maximum angular ranges  $\alpha_M$  and  $\beta_M$  can be found using trigonometric approaches. The former, as already derived in [5], is found as twice the angle between the triangle's hypotenuse ( $nd_c$ ) and the side  $(r-r_d)$ :  $r-r_d = nd_c \cos(\alpha_M/2)$  thus,

$$\alpha_M = 2 \arccos\left(\frac{r-r_d}{nd_c}\right), \quad r \geq r_d. \quad (17)$$

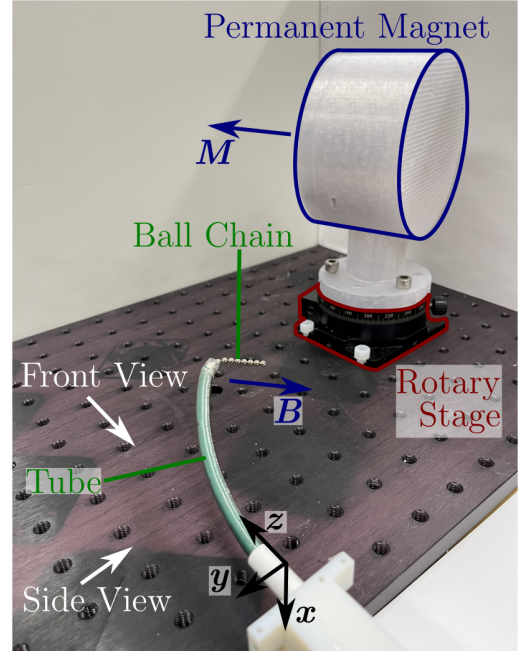


Fig. 4: Experiment set up for Front View magnetic field rotations about the  $x$  axis.

Notice that, in this case, we could assume the triangle is a right triangle. On the contrary, in Fig. 3(b), this assumption is not valid, in general, and we use the law of cosines:  $r_d^2 = r^2 + n^2 d_c^2 - 2r n d_c \cos(\beta_M/2)$ . We obtain the angular range

$$\beta_M = 2 \arccos\left(-\frac{r_d^2 - r^2 - n^2 d_c^2}{2r n d_c}\right), \quad r \geq r_d. \quad (18)$$

#### V. EXPERIMENTAL VALIDATION

We conducted experiments to validate the kinematic model of Section II and to demonstrate the dexterous workspace derived in Section IV. The data was collected using the setup in Fig. 4, consisting of two orthogonal cameras (webcam

C920, Logitech, US) placed in the directions of the front and side views as labeled.

The tendon-actuated tube was 10.16cm (4 inch) long with the tendon positioned upwards (in the  $x$  direction). The tube is composed of two layers: an inner layer of PTFE (polytetrafluoroethylene), an outer layer made of PEBAX (a modified polyamide). A braid made of Stainless Steel 304, is placed between them. The tendon runs the entire length between the outer layer and the braid.

The ball chain was composed of ten N42 magnetic spheres of diameter 3.175mm (1/8inch), mass 0.13g and remanence 1.32T (K&J Magnetics, USA). An external N52 cylindrical magnet (76.2mm diameter, 38.1mm long, 1.48T remanence) was mounted on a rotatory stage so that it could be precisely positioned with respect to the robot, and its dipole direction could be precisely controlled.

The tube was loaded with no load (0Kg), medium load (0.4Kg) and max load (1.4Kg), by hanging weights over pulleys at the proximal end of the tendon. The maximum load was selected to achieve a bending angle of  $90^\circ$  at the tube's tip. We repeated the experiments with the same loads while extending ball chains of four and eight balls, and rotating the external magnet to four orientations:  $\pm y$ ,  $\pm z$ . The overall set of data used for validation included 24 different configurations. We also collected data (three repetitions) with the tube without internal magnetic balls and used it to compute the elastic modulus of the tube, found to be approximately 4.10GPa, and a shear modulus of 34.13MPa. The tube was observed to retain a radius of curvature of 56.4mm when the tendon load was removed. Also, the plane of bending differed from the anticipated vertical plane by an angle of  $-26.8^\circ$  rotation around the  $z$  axis from the  $x$  direction. These parameters were estimated by tracking the tube's center line using the orthogonal set of webcams.

The tubes' center line was extracted from the images using the *active contour* and *skeletonizing* operations from the Matlab Image Processing Toolbox. The position of each ball was found using *imfindcircles*. The data was converted from the image space to the world space by calibrating each camera using the Matlab *camera calibrator* app; the calibration error was found to be of 1.20px for the front camera and 1.46px for the side camera.

### A. Kinematic Model Evaluation

We evaluated the kinematic model of Section II by comparing the experimental data with model predictions. To assess the assumption that the ball chain does not affect tube shape, we computed the error for both tube tip position and ball chain tip position.

While the tube's centerline was accurately extracted from the images as described above, the tip of the tube was not accurately identified from the images. In contrast, the centers of all extended balls were accurately determined. Therefore, we used the center position of the proximal extended ball as a proxy for tube tip position in order to compute tube modeling error. The center position of the distal ball was

TABLE I: Kinematic Modeling Error. Percentage is tip error normalized by robot length.

	Tube Model	Total Model
Mean Error	3.7mm (3.8%)	4.4mm (3.0%)
Max Error	4.9mm (5.0%)	8.7mm (7.0%)

used to assess overall error in the combined tube and ball chain model.

Table I reports the mean and maximum modeling errors for the tube and total models. We also include the errors as percentages normalized with respect to the tube's (Tube Model) and total robot's (Total Model) length. Mean errors of 1.5-3% of length have been reported for other types of continuum robots [6]. Given that our model assumes constant curvature tube bending and no tube deflection from the ball chain, a total model mean error of 3% is quite good. For clinical use, the maximum error is perhaps the more important quantity to consider and a value of 8.7mm for a 132mm long robot could be too large for some applications. (See Fig. 5 for depictions of minimum and maximum error configurations.)

To improve the accuracy, a coupled model that includes deflection of the tube due the ball chain is likely to substantially reduce the error. This can be inferred by comparing the tube and total model errors in Table I. The mean error in the tube model represents 84% of the total model error. In addition, during the experiments, deflection of the tube was observed during motion of the external permanent magnet.

### B. Dexterous Workspace Demonstration

To assess the dextrous workspace of the hybrid design as shown in Fig. 3, we placed a target in the dextrous portion of the workspace located along the main axis ( $z$ ) of the catheter, and displaced 25mm upwards (axis  $-x$ ). We then positioned the robot such that the tip touched the target from directions ranging over  $2\pi$  in the front and side view planes.

Four configurations of the front view are shown in Fig. 6(a) that are spaced roughly  $\pi/2$  apart illustrating that  $\beta_M = 2\pi$ . Note that the hybrid robot can rotate continuously through this angle range.

In contrast, the side view configurations (Fig. 6(b)) experience a geometric constraint in that the ball chain cannot pass physically through the curved tube. While  $\alpha_M = 2\pi$ , this results in a tip tangent angle, as shown in Fig. 6(b) ① and ②, that can be approached from either above or below. The tip tangent cannot, however, move continuously through this value, but instead has to switch from ball chain up to ball chain down or vice versa by passing through the configuration of Fig. 6(b) ③.

Figure 6 demonstrates that the hybrid continuum robots proposed here do have a dextrous workspace, even if the external magnetic field does not always suffice to fully straighten the ball chain as is assumed by the model of Section IV. This provides the capability for the robot to approach points in its dextrous workspace from all possible directions.

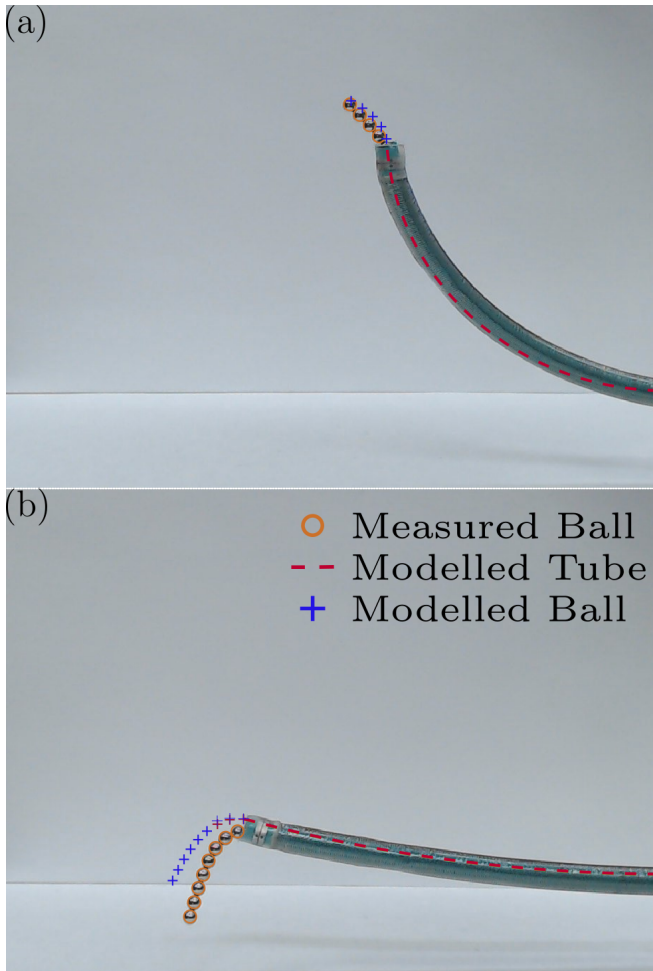


Fig. 5: Side view experimental results for configurations with (a) smallest error; (b) largest error.

## VI. CONCLUSIONS

In the present paper, we introduced a novel concept for designing continuum robots to produce a dexterous workspace. This hybrid approach combines a tendon-actuated proximal sheath with a distal telescoping magnetic ball chain controlled using an external magnet.

While a complete mechanics-based model is outlined, the paper develops a simpler model that enables sequential solution of tube shape followed by ball chain shape. The simpler model is tested experimentally and shown to provide normalized mean tip error comparable to other published physics-based continuum robot models.

For evaluating workspace dexterity, we also describe a further simplified kinematic model that treats the sheath as constant curvature and the ball chain as linear. This results in a closed-form solution for the forward and inverse kinematics. Experiments confirm the validity of our dexterity analysis.

Future work will evaluate feedforward and feedback control of these hybrid designs. This will include a comparison of simplified and coupled mechanics-based models as well as the application of the system to potential clinical tasks.

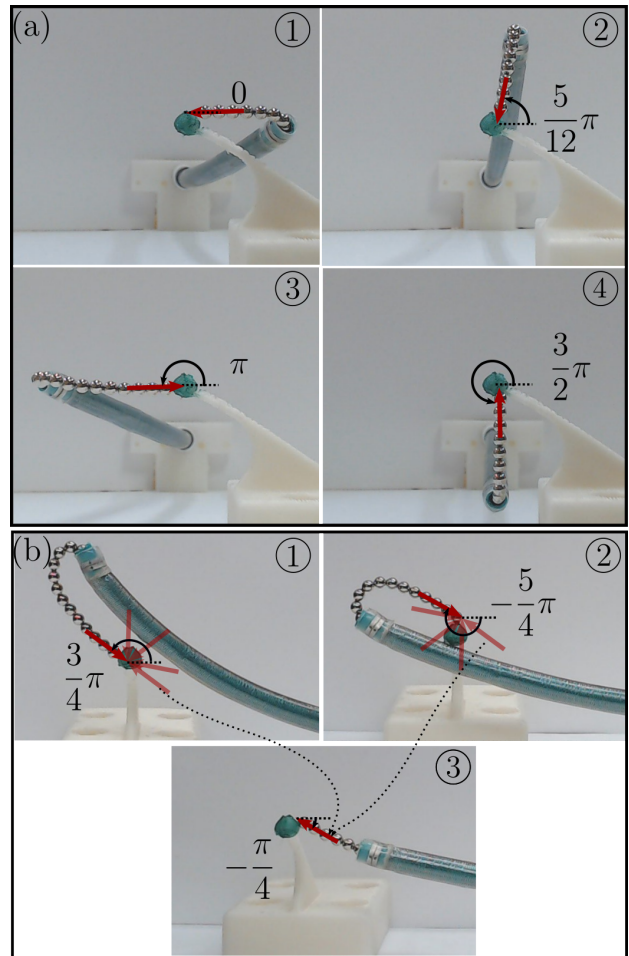


Fig. 6: Assessing tip dexterity. (a) Front view configurations spaced  $\sim \pi/2$  apart illustrating that  $\beta_M = 2\pi$ . (b) Side view configurations. While  $\alpha_M = 2\pi$ , side view tip approach angles are grouped into ball chain down ① and ball chain up ② configurations depicted here at their common tip tangent boundary. The red arrows indicate the range of tip tangent angles associated with each set. To switch from one set to the other, it is necessary to pass through configuration ③.

## REFERENCES

- [1] P. Dupont, N. Simaan, H. Choset, and C. Rucker, "Continuum Robots for Medical Interventions," *Proceedings of the IEEE*, 2022.
- [2] D. C. Rucker and R. J. Webster, "Statics and dynamics of continuum robots with general tendon routing and external loading," *IEEE Transactions on Robotics*, vol. 27, no. 6, pp. 1033–1044, 2011.
- [3] G. Pittiglio, M. Mencattelli, and P. E. Dupont, "Magnetic ball chain robots for endoluminal interventions," in *2023 IEEE International Conference on Robotics and Automation (ICRA)*, 2023, pp. 4717–4723.
- [4] K. O'Donoghue and P. Cantillon-Murphy, "Deflection modeling of permanent magnet spherical chains in the presence of external magnetic fields," *Journal of Magnetism and Magnetic Materials*, vol. 343, pp. 251–256, 2013.
- [5] G. Pittiglio, M. Mencattelli, and P. E. Dupont, "Closed-form kinematic model and workspace characterization for magnetic ball chain robots," in *2023 International Symposium on Medical Robotics (ISMR)*, 2023, pp. 1–7.
- [6] R. M. Grassmann, R. Z. Chen, N. Liang, and J. Burgner-Kahrs, "A dataset and benchmark for learning the kinematics of concentric tube continuum robots," in *2022 IEEE/RSJ International Conference on Intelligent Robots and Systems (IROS)*, 2022, pp. 9550–9557.